

A New InP/InGaAs Double Heterojunction Bipolar Transistor (DHBT) With a Step-Graded InAlGaAs Collector Structure

Tzu-Pin Chen, Shiou-Ying Cheng¹, Ching-Wen Hung, Kuei-Yi Chu, Li-Yang Chen, Tsung-Han Tsai, and Wen-Chau Liu*

Institute of Microelectronics, College of Electrical Engineering and Computer Science, National Cheng Kung University

¹Department of Electrical Engineering, National Ilan University

Email: wcliu@mail.ncku.edu.tw

IEEE Electron Device Letters, Vol. 29, No. 1, pp. 11-14, Jan 2008.

Over the past years, InGaAs-based heterojunction bipolar transistors (HBTs) have attracted significant interest for microwave and low-power digital applications due to excellent transport properties of the InGaAs material. However, the intrinsic disadvantage of low breakdown voltage and high output conductance limit their applications in low-voltage and low-power dissipation digital circuits. On the other hand, double heterojunction bipolar transistors (DHBTs) have been used to improve the breakdown characteristics. Nevertheless, for DHBTs, an abrupt heterojunction at the B-C interface induces a large degradation of device performance caused by the current blocking effect. To overcome this problem, several approaches have been reported, such as p-n pair, composite collector structure, and a compositionally graded layer at the base-collector (B-C) junction to form the improved double heterojunction structures.



In this work, an interesting InP/InGaAs HBT with a step-graded InAlGaAs collector structure is presented and studied. The step-graded collector uses a quaternary InAlGaAs material between base and collector layer. In addition, the potential spike between base and collector layer can be effectively reduced due to the presence of this inserted quaternary InAlGaAs material. The quaternary InAlGaAs step-graded collector structure is composed of several graded layers with different energy band gaps. This variable band lineup is increased from base to collector layer. Due to the effectively larger bandgap of the composite collector structure, a larger collector breakdown electric field (voltage) can be expected.

The simulated energy band diagrams near the B-C junction of the conventional DHBT and the studied device at thermal equilibrium are shown in Fig. 1. The distribution of the base-collector barrier in the depleted collector region makes it possible for electrons with sufficient kinetic energy to transport over the conduction band spikes even at zero bias. The presence of the InGaAs setback layer near to the P⁺ InGaAs base is beneficial in minimizing the carrier blocking effect. Basically, this layer suspends the extension of the first conduction band spike into the base-collector space charge region, which can substantially block electrons transiting into the collector. Furthermore, the originally high and wide spike presented at the base/collector interface can be separated into some low and narrow spikes when the step-graded InAlGaAs layers are inserted between base-collector heterointerface. Therefore, the

improvement of collection efficiency of electrons can be obtained.

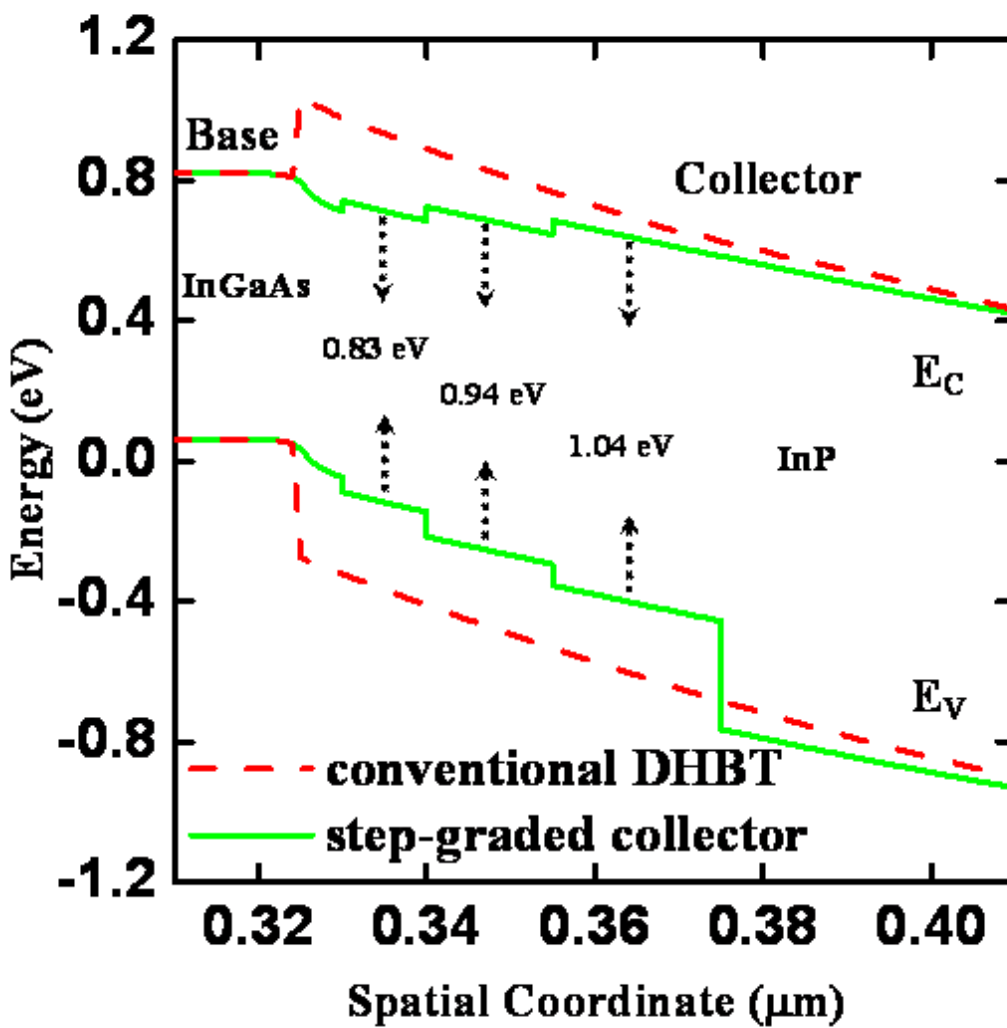


Fig. 1 The energy band diagram near the B/C junction of the conventional DHBT and the studied step-graded collector structure at thermal equilibrium.

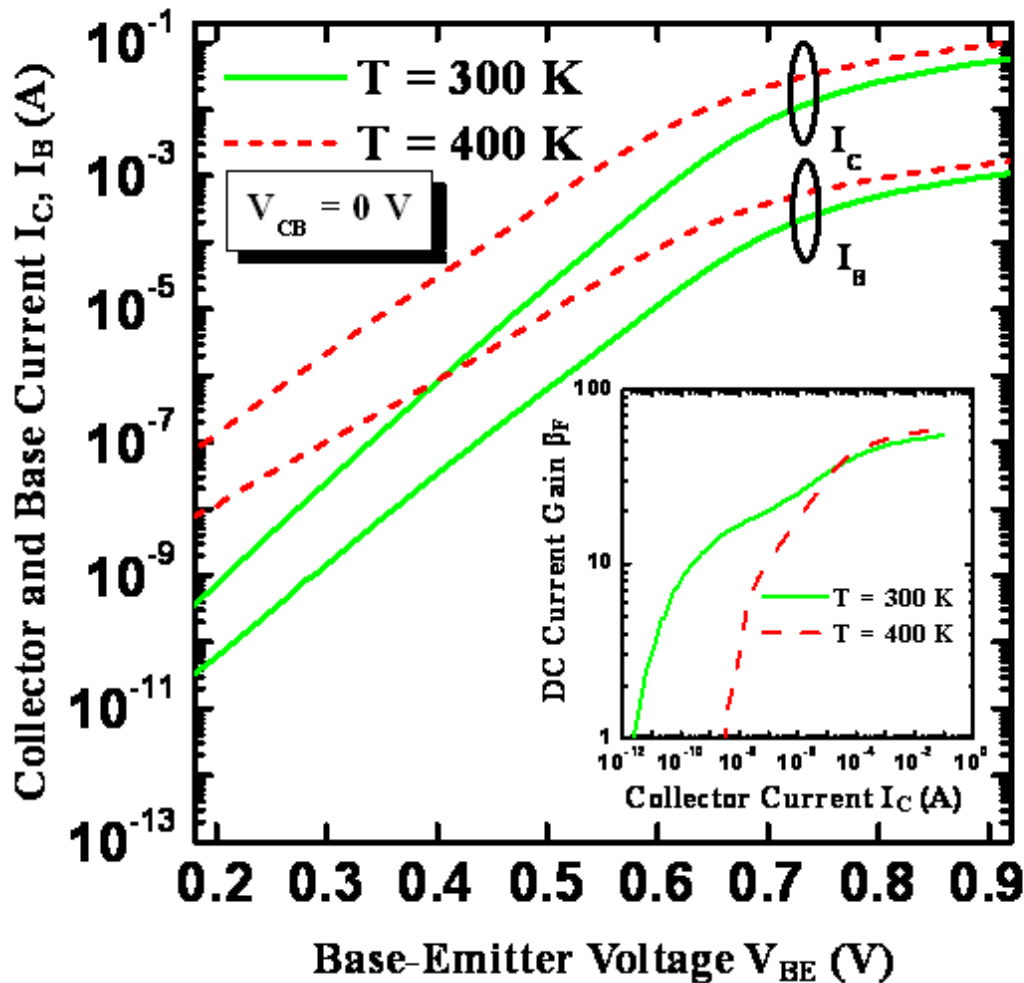


Fig. 2 The Gummel plots of the studied device at 300 and 400 K. The dependences of DC current gain β_F on the collector current I_C at 300 and 400 K are shown in the inset.

Figure 2 shows the Gummel plots of the studied DHBT measured at 300 and 400 K. The collector-base voltage is kept at $V_{CB} = 0$ V. The ideality factors of collector (base) current are 1.15 (1.27) and 1.1 (1.22) at 300 and 400 K, respectively. The ideality factor is primarily discussed by carrier transport on the conduction band at emitter/base (base/collector) junction. The 1-kT like collector current I_C indicates that the transport of conducting carrier is primarily dominated by the thermionic emission and diffusion mechanisms. The slightly deviation of n_C value from unity is mainly attributed to the tunneling current through the B-E (B-C) heterojunction. In addition, the decrease of n_C with elevating the temperature indicates the substantial importance of thermionic emission at higher temperature. The near unity of n_B value reveals that the bulk recombination current dominates the whole base current especially at higher temperature. Clearly, this good performance of ideality factors is directly related to the use of step-graded collector heterostructure. Furthermore, the studied device exhibits the low offset and saturation voltage of 98.4 mV and 0.33 V. Furthermore, the dependences of dc current gain β_F on the collector current I_C at 300 and 400 K are shown in the inset of Fig. 2. The collector-base voltage is fixed at $V_{CB} = 0$ V. The studied device can be operated under extremely wide collector current regimes. The operation regime is wider than 11 decades in magnitude of collector current ($I_C = 10^{-12}$ A to $I_C = 10^{-1}$ A). Experimentally, the current gain β_F of the studied device is greater than unity even at an extremely low

collector current of $I_c = 2.3 \times 10^{-12}$ A at 300 K. The observation of β_f at the extremely low current region is mainly caused by the insertion of the step-graded InAlGaAs collector structure. This step-graded InAlGaAs collector structure effectively reduces the potential spike at B-C heterointerface. Moreover, the higher dc current gain at 400 K is found as the collector current is increased to $I_c = 10^{-4}$ A. It is attributed to the high thermal collector leakage current with increasing the temperature. This gives a great contribution to the collector current I_C and results in higher dc current gains.

Figure 3 illustrates the typical common-emitter I-V characteristics of the studied device at 300 and 400K. Obviously, the device shows high common-emitter breakdown and low output conductance. As the temperature is increased, carriers within the collector region obtain more thermal energy and thus increase the probability of impact ionization. Hence, the contribution of thermal generation apparently plays a key role in the increase of collector current I_C . Experimentally, the common-emitter breakdown voltage of our studied device with the collector thickness of 400 nm, at $I_c = 100 \mu\text{A}$, is 8.05 V. Moreover, our studied device has a lower offset and saturation voltage, which certainly leads to a larger voltage operation range. When the temperature is elevated, the raised collector current arising from the positive temperature dependence of impact ionization coefficient in the collector causes the lower breakdown voltage. Moreover, the studied device shows nearly identical amplification even at the temperature up to 400K. These superior characteristics again indicate the potentiality of the studied device in practical circuit applications.

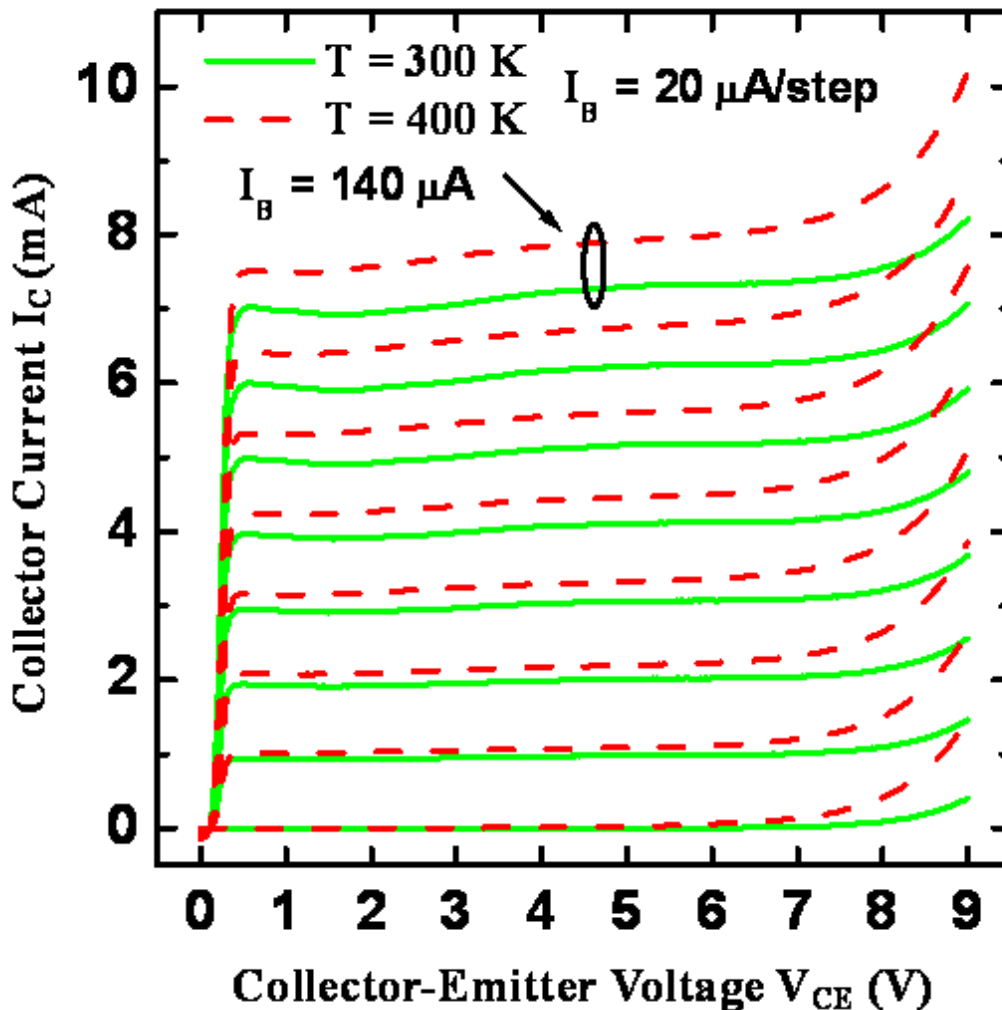


Fig. 3 Common-emitter current-voltage characteristics of the studied device at 300 and 400 K.

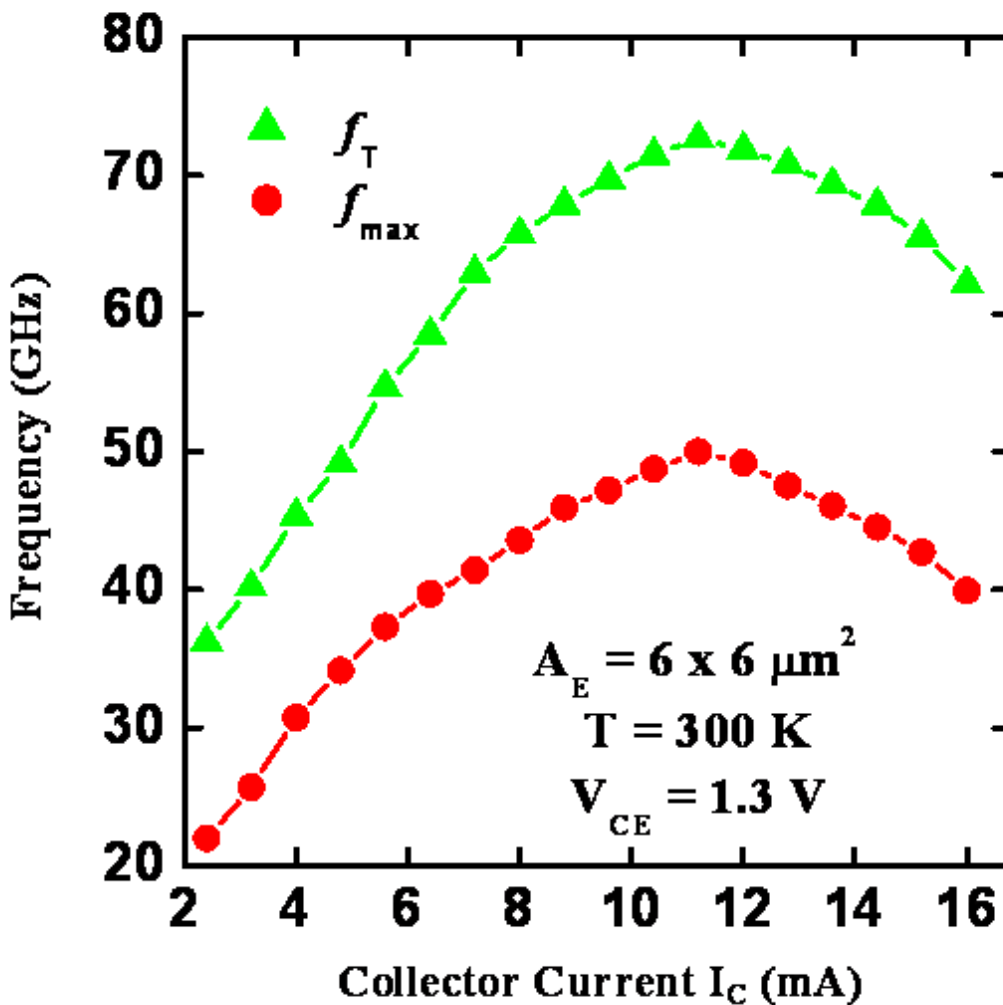


Fig. 4 Unity current gain cut-off frequency f_T and maximum oscillation frequency f_{max} versus collector current I_C for the studied device.

Figure 4 shows the dependences of unity current gain cut-off frequency f_T and maximum oscillation frequency f_{max} as a function of collector current I_C . For a nonoptimized device ($A_E = 6 \times 6 \mu\text{m}^2$), the peak f_T (f_{max}) of the studied device is 72.7 GHz (50 GHz). Clearly, due to the employment of the step-graded collector structure, the studied device exhibits excellent microwave characteristics. The fall-off phenomena of f_T and f_{max} at high collector current regions are caused by the Kirk effect and series resistance effect.

In conclusion, the dc and microwave characteristics of an interesting InP/InGaAs DHBT with a step-graded InAlGaAs collector structure are studied and demonstrated. Based on the employment of the step-graded InAlGaAs collector structure at the B-C heterojunction, the undesired electron blocking effect can be eliminated. Experimentally, the operation regime is wider than 11 decades in magnitude of collector current ($I_C = 10^{-12}$ A to $I_C = 10^{-1}$ A). Furthermore, the studied device shows a relatively high common-emitter breakdown voltage and low output conductance though at high temperature. Good

values of f_T (72.7 GHz) and f_{max} (50 GHz) have been obtained for a nonoptimized device.

References

- [1] J. Y. Chen, D. F. Guo, S. Y. Cheng, K. M. Lee, C. Y. Chen, H. M. Chuang, S. Y. Fu, and W. C. Liu, "A new InP–InGaAs HBT with a superlattice collector structure," *IEEE Electron Device Lett.*, vol. 25, no. 5, pp. 244–246, May 2004.
- [2] W. K. Huang, S. C. Huang, H. W. Chung, Y. M. Hsin, J. W. Shi, Y. C. Kao, and J. M. Kuo, "37-GHz bandwidth monolithically integrated InP HBT/evanescently coupled photodiode," *IEEE Photon. Technol. Lett.*, vol. 18, no. 12, pp. 1323–1325, Jun. 2006.
- [3] J. H. Tsai and Y. C. Kang, "DC performance of InP/InGaAs p-n-p heterostructure-emitter bipolar transistor," *IEEE Trans. Electron Devices*, vol. 53, no. 5, pp. 1265–1268, May 2006.
- [4] N. Parthasarathy, Z. Griffith, C. Kadow, U. Singiseti, M. J. W. Rodwell, X. M. Fang, D. Loubychev, Y. Wu, J. M. Fastenau, and A. W. K. Liu, "Collector–pedestal InGaAs/InP DHBTs fabricated in a single-growth, triple-implant process," *IEEE Electron Device Lett.*, vol. 27, no. 5, pp. 313–316, May 2006.
- [5] A. Feyngenson, D. Ritter, R. A. Hamm, P. R. Smith, P. K. Montgomery, R. D. Yadvish, H. Temkin, and M. B. Panish, "InGaAs/InP composite collector heterostructure bipolar transistors," *Electron. Lett.*, vol. 28, no. 7, pp. 607–609, Mar. 1992.

Copyright 2009 National Cheng Kung University

Strategies for functional validation of genes involved in reproductive stages of orchids

Ming-Hsien Hsieh, and Hong-Hwa Chen*

¹Department of Life Sciences, and ²Institute of Biotechnology, National Cheng Kung University, Tainan 701, Taiwan

Email: hhchen@mail.ncku.edu.tw

Plant Physiology 143: 558-569 (2007)

Orchids have profound diversity of specialized pollination and ecological strategies. Hence, orchid is ideal plant species to study molecular evolution and functional genomics. The sophisticated orchid flower morphology includes two whorls of perianth segments, three sepals and three petals, one of the petals is modified as labellum (or lip). In addition, the male and female reproductive organs are fused to form a gynostemium. The diversity and specialization in orchid floral morphology have fascinated botanists and collectors for centuries.

Phalaenopsis is a member of the *Orchidaceae*, one of the largest families of flowering plants. *Phalaenopsis* industry has been developed as an international leading agricultural industry in Taiwan. FloraCulture International (2002) has reported that regarding world trade, the largest orchid plant exporter is Taiwan. Furthermore, *Phalaenopsis* has been selected by Council of Agriculture as one of the four key representative agricultural products in Taiwan. Thus, there is no need to emphasize how important *Phalaenopsis* is. The research on *Phalaenopsis* not only can offer the opportunity to answer the diversity and specialization in orchid biology, but also provide a basis for crop improvement to enhance the competition capability in *Phalaenopsis* industry worldwide.



Forward and reverse genetics are two methods used to determine gene function. Forward genetics starts with random mutagenesis of an entire genome, after which the trait selection is followed to identify the mutated gene or genes. Reverse genetics disrupts gene expression to search for a phenotype usually beginning with cloned DNA sequences. The problems with forwards genetics include the long life-cycle and lack of high-resolution genetic maps in orchids. The problems with the reverse genetic methods using T-DNA insertion or transposon-tagging include difficulties in plant transformation and long regeneration time in orchids. Here we describe a new approach facilitated by virus-induced gene silencing (VIGS) to accelerate the analysis of orchid gene function.

Virus-induced gene silencing is highly effective at detecting candidate gene function. To carry out VIGS, a fragment of the target gene is cloned into a virus vector. As the virus vector inoculates, the target gene replicates and spreads in the plant. The plant responds with RNA interference as a defense mechanism. The virus vector containing the heterologous insert and their mRNA suffer degradation. This causes a down-regulation of the target gene and often cases a clear phenotype develops. The advantages of VIGS

include the short-time required for down-regulation of the target gene and this may give us the ability to study essential genes. VIGS is much easier and more efficient at overcoming functional redundancy by effectively suppressing all or most genes in a given family.

Of all the current viral vectors used in VIGS, potato virus X (PVX) and Tobacco mosaic virus (TMV) are successful VIGS vectors in potato and tobacco respectively. Both PVX and *Cymbidium* mosaic virus (*CymMV*) belongs to the same genus, and both TMV and *Odontoglossum* ringspot virus (ORSV) belongs to the same genus. Thus, *CymMV* and ORSV are orchid viruses that can be considered as VIGS vectors. After screening, the highly prevalent orchid virus *CymMV* was chosen as a VIGS vector, which does not induce any symptoms. This vector successfully induced gene silencing by knocking down the RNA levels of *Phytoene desaturase* (*PDS*) gene in the leaves by 54% in less than 2 months confirming that this virus vector can be used in the study of *Phalaenopsis*.

Under normal circumstances orchids bloom from March to May, but we need them to bloom throughout the year in order to efficiently study their reproductive stage. In order to allow for regular blooming, a grow chamber is required. Commercial orchid growers recommend that orchids be kept at 25 °C during the day and at 20 °C at night with the correct humidity and fertilization that can stimulate stalks for flowering. In order to show that the *CymMV* vector can induce silencing in all flower organs we use a B-class MADS-box gene, *PeMADS6* which are transcribed in all of the flower organs. We selected a stretch of 150 nucleotides (nts) from the less conserved 3'-terminus, and inserted it into the *CymMV* vector, and named it as p*CymMV*-pro60-*PeMADS6*IR. The flowers blossomed six weeks post inoculation of the 6-node emerging stalks of *P. amabili* var. *formosa*. Reduced *PeMADS6* RNA levels to 63±2%, 33±3%, 23±5% and 33±2% were detected in sepals, petals, lips and columns, respectively in the plants inoculated with p*CymMV*-pro60-*PeMADS6*IR as compared to the mock-inoculated plants. To confirm whether the reduced expression of *PeMADS6* was due to RNA interference mediated by VIGS, small-molecular-weight RNA was purified from the inoculated plants and then performed northern blot hybridization with probes containing either *CymMV* Coat protein (*CP*) gene or *PeMADS6* gene. The *CymMV* CP probe could detect 21-nt small interfering RNA (siRNA) in both the mock-inoculated plant as well as plants inoculated with p*CymMV*-pro60-*PeMADS6*IR. However, it could only detect the 21-nt siRNA of *PeMADS6* in the plants inoculated with p*CymMV*-pro60-*PeMADS6*IR.

In addition, these plants inoculated with p*CymMV*-pro60-*PeMADS6*IR showed modified phenotype with several morphological changes. These include streaks or patches of greenish tissue were observed in the sepals, petals and lips. Another interesting change was the initial inability of flower buds to blossom on the lower stalks of inoculated plants. The flower buds were able to blossom on the upper stalks, but did so with streaks or patches of greenish tissue in the sepals, petals and lips. After dissecting the initial flower buds on route to abort, fully formed sepals, petals, lips and columns were found within these plants similar to healthy plants. This indicates that reduced transcript levels of MADS-box family genes still allowed initial flower development to occur normally, but it was insufficient for further development and blossoming to occur.

Interestingly, similar results were obtained when the experiments were conducted in another two orchid varieties, *P. amabilis* and *P. Sogo Musadium*. Both varieties are tetraploid, and in general, loss-of-function assays are not easy to perform in plants with multiple copies. With loss-of-function assays, such as T-DNA insertion or transposon tagging, simultaneously targeting all genes with functional redundancy is difficult. In contrast, VIGS can knock down the RNA level after RNA transcription, regardless of the RNAs transcribed from genes in different genome locations, and thus can silence all genes simultaneously.

These results demonstrate that the newly constructed *CymMV*-based vector is suitable for analyzing genes involved in the floral morphogenesis of *Phalaenopsis* spp. As *CymMV* has a wide host range among various genus of *Ochidaceae*, including *Phalaenopsis*, *Cymbidium*, *Cattleya*, *Dendrobium*, *Epidendrum*, *Laelia*, *laeliocattleya*, *Oncidium*, *Zygopetallum*, *Vanilla*, and *Vinda*, the developed vectors will contribute well to functional genomics studies of these orchids. With the advent of genomics and bioinformatics, the past few years have seen great strides in the amount of gene information available and development of tools for their analysis of orchids. Thus, the *CymMV*-based vector can be used for the functional validation of genes in orchids, to overcome their large genome size, low transformation efficiency, long regeneration time, and long life-cycle.

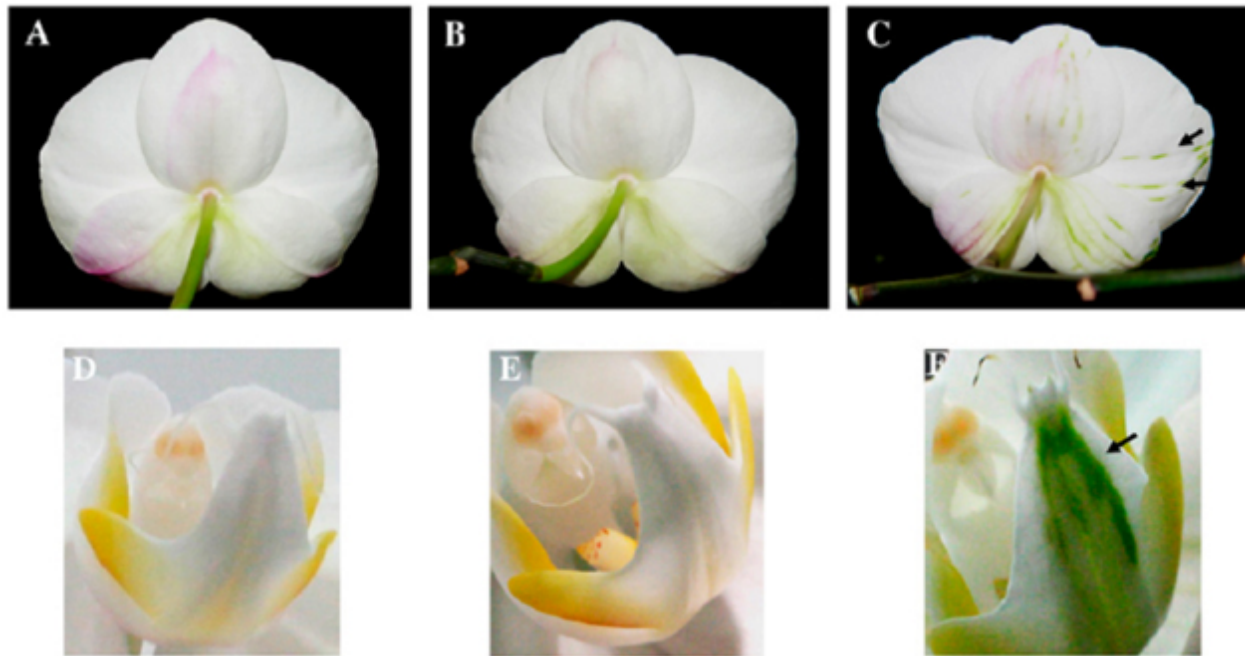


Figure 1. Phenotype on MADS-box gene-silenced plants. Plants of *P. amabilis* var. *Formosa* were infected with buffer (A and D), p*CumMV*-pro60 (B and E), or p*CymMV*-CP60-*PeMADS6* (C and F). The arrows on C indicate greenish streaks of the flower and those on F indicate greenish patches of the lip.

On Students' Strategy-Preferences for Managing Difficult Course Work

Hua-Li Jian^{1*}, Frode Eika Sandnes², Yo-Ping Huang³, Cai Li⁴ and Kris Law⁵

¹Dept. of Foreign Languages and Literature, National Cheng Kung University, Taiwan

²Oslo University College, Norway

³National Taipei University of Technology, Taiwan

⁴Communications University of China, PRC

⁵City University of Hong Kong, Hong Kong

Email: huali.jian@gmail.com

IEEE Transactions on Education, Vol. 51, No. 2, pp. 157-165, May 2008.

Well-designed course work stimulates students' learning processes (learning by doing). Teachers have to carefully adjust the course work difficulty level. Students need challenges of sufficient difficulty for academic development to occur. Still, the course work must not be so difficult that it can be completed only by the upper quartile of students. Course work perceived by students to be too difficult is more likely to push students into pursuing undesirable strategies for reaching their goals, compared to course work where students perceive they are in control.



This study investigates how students respond to assignments and course work that are too difficult. In particular, which strategies do they choose for overcoming the problem? Seven strategies are studied, namely, to seek legitimate help from the teacher or teaching assistants, questionable practices such as posting questions on Internet discussion forums or collaborating with fellow students to solve the problem, and totally unacceptable practices such as copying the assignments from fellow students, dividing the workload, searching for and adopting assignments on the Internet, or unjustifiably asking for extension based on a false doctor's note. Insight into how students rank various practices for handling difficult assignments is important when one wishes to deploy countermeasures to eliminate unacceptable practices and promote ethical practices.

Furthermore, the problem is also inspected from the reverse angle – namely, how do students who have completed their course work respond to requests for help from fellow students? Six strategies for managing requests for help are studied, namely, to point the students in the right direction, let the students look at their own course work, let the students copy their course work, inform the teacher of the students, ignore the students altogether, or provide the students with erroneous advice. Insight into how students respond to requests for help from other students is, therefore, important when establishing ethical guidelines and working practices for an educational program.

Another important issue is how students rank the various stakeholders in the educational environment. Are the teacher and the university really at the top of this hierarchy, or do students have a different

perspective on who is more important? Students, just as all other people, are occasionally faced with ethical dilemmas. In particular, they may be drawn into a problematic situation where they have to make a choice. Should they take the side of the student with whom they may feel empathy or the teacher who enforces class justice and ensures overall fairness? To shed light on this issue, the final part of this study addresses how students choose sides in a situation of conflict. The five most distinctive stakeholders in the educational environment are included, namely, the students themselves, their friends, their parents, their teachers, and their institution.

Data acquired through a questionnaire issued to students were analyzed using a pair-wise comparison method. This robust method allows the overall student preferences to be ranked statistically. Data, based on the responses of 233 students, is drawn from student populations in four cultural regions across two continents, including both undergraduate and postgraduate students, to get a more global perspective. Most of the participants were engineering students. In addition, 57 humanities students were included for reference.

Table 1: Students' preferences for managing difficult course work are listed in terms of their normalized ranking coefficient with the actual rank in parenthesis. Listed is also the agreements U among the respondents, the χ^2 statistics, and the corresponding p-values (df=21). UG = undergraduates, PG = postgraduates.

Description	Engineering							Humanities	
	Hong Kong	China		Norway	Taiwan			UG	PG
	UG+PG	UG	PG	UG+PG	UG (1yr)	UG (3-4yr)	PG	UG	PG
Ask teacher (w_1)	0.14 (4)	0.13 (4)	0.11 (6)	0.15 (4)	0.09 (6)	0.10 (6)	0.09 (6)	0.11 (5)	0.15 (4)
Solve problem with friend (w_2)	0.24 (1)	0.24 (1)	0.18 (2)	0.22 (1)	0.22 (1)	0.22 (1)	0.23 (1)	0.24 (1)	0.22 (2)
Post question on Internet discussion group (w_3)	0.12 (5)	0.12 (5)	0.17 (3)	0.15 (5)	0.12 (5)	0.13 (4)	0.11 (5)	0.12 (4)	0.11 (5)
Search for solution on the Internet (w_4)	0.20 (2)	0.20 (2)	0.24 (1)	0.22 (2)	0.20 (2)	0.22 (2)	0.23 (2)	0.20 (3)	0.24 (1)
Copy and change friends assignment (w_5)	0.08 (6)	0.09 (6)	0.12 (5)	0.03 (6/7)	0.16 (4)	0.11 (5)	0.11 (4)	0.04 (7)	0.03 (7)
False doctor's note (w_6)	0.03 (7)	0.03 (7)	0.02 (7)	0.03 (6/7)	0.02 (7)	0.03 (7)	0.03 (7)	0.06 (6)	0.06 (6)
Divide the work with friends (w_7)	0.19 (3)	0.18 (3)	0.16 (4)	0.20 (3)	0.20 (3)	0.20 (3)	0.20 (3)	0.22 (2)	0.20 (3)
Agreement U	0.39	0.36	0.33	0.45	0.39	0.39	0.46	0.45	0.51
χ^2 (df=21)	201.2	242.5	130.8	78	348.5	276.3	260.6	284.9	310.3
p	<0.01	<0.01	<0.01	<0.01	<0.01	<0.01	<0.01	<0.01	<0.01

The students seem to have similar preferences for handling difficult course work irrespective of geographical origin, level of study, and field of study (Table 1). All groups prefer to ask a friend for help if they have difficulties ($w_2=0.22-0.24$, rank 1/7), with the exception of the Mainland Chinese postgraduates and the Taiwanese humanities postgraduates who prefer to search for a solution on the Internet ($w_4=0.24$, rank 1/7). Surprisingly, all groups prefer other alternatives than actually asking the teacher for help. Four groups rank the teacher second last ($w_1=0.09-0.11$, rank 6/7), and four groups rank help from the teacher in fourth place ($w_1=0.13-0.15$, rank 4/7). Why are the teachers ranked this low, especially as teachers' chief purpose is to supervise and guide students? Perhaps teachers' perception of their own supervisory value is overrated? Teachers often complain about the effort involved when supervising students. Usually, just a fraction of students actually seek help from the teacher. These students often demand considerable help, and the teachers may perceive from their effort that they have done their part adequately. However, what happens to all the others, i.e., the majority, who do not seek help from the teacher? Do they not have any difficulties? They may be trying other alternatives instead.

Most groups, with the exception of the humanities students and the Mainland Chinese postgraduates,

rank searching for solutions on the Internet in second place ($w_4=0.20-0.23$, rank 2/7). Searching for a solution on the Internet is not an acceptable strategy unless the students only seek out additional information that will help them understand the problem and consequently solve the assignment. Clearly, the Internet has greatly changed students' working habits and approach to problem solving compared to 15 years ago, since most universities then did not use the Internet for much besides e-mail and newsgroups. Teaching practices and views of the learning processes have perhaps not changed at the same pace. Many students are likely to resort to Internet search engines for any research and referencing need. Students, therefore, need to be trained in ethical Internet working practices because the Internet is also an important tool in their subsequent professional careers.

The third preference on most groups' list was to divide the work among friends ($w_7=0.18-0.20$, rank 3/7), undeniably an unacceptable, but common practice. Students pressed for time divide assignments among themselves so that, for instance, a student good at mathematics will do the mathematics assignment, the computer-wiz will do the programming assignments, and so on. They then share the results afterwards. Unfortunately, the students who are weak in mathematics will not gain any training and lose their chance to improve their mathematics since their assignments have been done for them. Strong pedagogical reasons exist for hitting down hard on this malpractice. Division of labor may be a common, and even essential, practice in industry; but when one receives credit for work that one has not done, then that credit is a form of plagiarism. The Mainland Chinese postgraduates and Taiwanese humanities undergraduates deviated from this pattern since the Mainland Chinese postgraduates ranked division of labor in fourth place ($w_7=0.16$, rank 4/7), while the Taiwanese humanities undergraduates ranked division of labor in second place ($w_7=0.20$, rank 2/7).

The practices of copying and changing a friend's assignment and asking for an extension using a false doctor's note are for most groups ranked in second to last ($w_5=0.03-0.09$, rank 6/7) and last ($w_6=0.03-0.06$, rank 7/7) place, respectively. Both of these practices are highly unethical. The low rank is a positive sign that students view these practices as a last resort. Perhaps asking for a doctor's note is too troublesome, may incur some expense, and may not always be possible (depending on the particular patient-doctor relationship and national practices). Most teachers receive doctors' notes that they suspect are not legitimate. Furthermore, copying a friend's assignment is also humiliating for a student, especially if he or she has to ask. The only exception was the Taiwanese humanities students who ranked using a false doctor's note in second to last place ($w_6=0.06$, rank 6/7).

Table 2. Handling requests from fellow students.

Description	Engineering							Humanities	
	Hong Kong	China		Norway	Taiwan			UG	PG
	UG+PG	UG	PG	UG+PG	UG (1yr)	UG (3-4yr)	PG	UG	PG
Ignore the request (w_1)	0.19 (3)	0.11 (4)	0.12 (4)	0.17 (3)	0.16 (3)	0.17 (3)	0.15 (4)	0.16 (3)	0.16 (3)
Point student in the right direction (w_2)	0.32 (1)	0.29 (1)	0.29 (1)	0.32 (1)	0.29 (1)	0.30 (1)	0.29 (1)	0.32 (1)	0.32 (1)
Let student look at your course work (w_3)	0.23 (2)	0.26 (2)	0.27 (2)	0.27 (2)	0.25 (2)	0.26 (2)	0.26 (2)	0.25 (2)	0.27 (2)
Allow student to copy (w_4)	0.10 (4)	0.18 (3)	0.15 (3)	0.14 (4)	0.18 (4)	0.15 (4)	0.17 (3)	0.10 (5)	0.09 (5)
Notify the teacher about the student (w_5)	0.08 (5)	0.10 (5)	0.11 (5)	0.06 (5)	0.05 (6)	0.07 (5)	0.06 (6)	0.15 (4)	0.14 (4)
Give erroneous advice (w_6)	0.07 (6)	0.05 (6)	0.05 (6)	0.04 (6)	0.07 (5)	0.05 (6)	0.08 (5)	0.03 (6)	0.02 (6)
Agreement U	0.49	0.43	0.46	0.68	0.45	0.52	0.45	0.59	0.66
χ^2 (df=15)	178.1	200.2	125.5	76.3	283.4	254.5	185.4	262.7	282.8
p	<0.01	<0.01	<0.01	<0.01	<0.01	<0.01	<0.01	<0.01	<0.01

The results in Table 2 show that the different groups generally agree regarding students' preferences for

responding to other students' requests for help. All groups declared that they first would try to point the student in the right direction ($w_2=0.29-0.32$, rank 1/6), followed by letting the students look at their own course work ($w_3=0.23-0.27$, rank 2/6).

The groups seem to be divided on whether the request should be ignored or whether they should allow their course work to be copied. The students with Western traditions, i.e., the Hong Kong students, Norwegian students, and most of the Taiwanese students prefer to ignore a request ($w_1=0.16-0.19$, rank 3/6), while the Mainland Chinese students prefer to let their course work be copied ($w_4=0.15-0.18$, rank 3/6); and they place ignoring the student in fourth place ($w_1=0.11-0.12$, rank 4/6).

Most groups rank informing the teacher about the student and giving the student erroneous information second last and last, respectively. Fortunately, most students reject the practice of spreading ill advice, although this practice is understandable from the students' perspective in very competitive environments. In some countries, such as Norway, government policy states that the grades must follow the normal distribution over a given window of time, where only 10% of the students are to receive A's, etc. Consequently, the students may adopt the spreading of ill advice as a survival practice since this strategy will increase their own chances of obtaining good grades. In fact, both the Taiwanese engineering sophomore and master students indicated a preference for giving bad advice to students ($w_6=0.07-0.08$, rank 5/6) rather than informing the teacher ($w_5=0.05-0.06$, rank 6/6). Surprisingly, informing the teacher is ranked in second to last place by most students ($w_5=0.05-0.11$, rank 5/6).

Copyright 2009 National Cheng Kung University

Phonon-assisted stimulated emission from pendeo-epitaxy GaN stripes grown on 6H-SiC substrates

Yun-Chorng Chang^{1*}, Yun-Li Li², Darren B. Thomson³, and Robert F. Davis³

¹Institute of Electro-Optical Science and Engineering, National Cheng Kung University

²Graduate Institute of Electro-Optical Engineering, National Taiwan University

³Department of Materials Science and Engineering, North Carolina State University

Email: ychang6@mail.ncku.edu.tw

Applied Physics Letter 91, 051109 (2007); Also Selected Article in Virtual Journal of Nanoscale Science & Technology 16(7) (2007)

III-Nitride semiconductors have emerged as the most promising materials in which to fabricate ultraviolet light emitting diodes and laser diodes. Uncoalesced stripes of GaN grown by pendeo-epitaxial (PE) lateral overgrowth technique exhibit parallel, atomically flat and mirror-like sidewalls with suspended, low dislocation density "wing" regions should form an ideal cavity with low scattering loss for stimulated emission. [Ref. 1] Stimulated emission located at one or more longitudinal optical (LO) phonon energies below the allowed quantum-well transition energies was first reported in AlGaAs/GaAs multiple quantum wells. [Ref. 2] Phonon-assisted recombination processes are stronger and easier to be observed in much polar materials such as GaN and II-VI materials.



In our previous work, phonon-assisted stimulated emission from a 13.3- μ m-wide PE-GaN stripe was demonstrated. [Ref. 3] Transverse-electric-polarized lasing with well-defined Fabry-Pérot modes was observed and located at one LO phonon (90 meV) below the bandgap of GaN. The effective refractive index of the GaN was calculated to be 8.578. This value is significantly higher than the value previously reported in the literature using ellipsometry [Ref. 4], which indicates that the absorption loss is more severe during lasing when the excess carrier concentration is very high.

The GaN sample investigated in this study was derived from a \sim 1.5 μ m thick GaN thin film that had been grown on a 100 nm AlN buffer layer previously deposited during the same growth run on a polished 6H-SiC (0001) substrate, lithography patterned, and etched using an Inductively coupled Cl plasma to form a set of GaN stripes on which was deposited additional GaN material that grew primarily along [1100] but without coalescence. The sample was mounted on a conductive copper plug and placed on the cold finger of liquid nitrogen Dewar. A frequency-quadrupled flash-lamp-pumped Nd:YAG laser having a pulse duration and repetition rate were 6 ns and 15 Hz, respectively, was used to acquire the photoluminescence (PL) spectra. The sample was illuminated at an angle slightly off the [0001] direction and oriented so that emission from the edge of the GaN stripes could be collected. The plan-view SEM image of four of the stripes is shown in Fig. 1(a) reveals that the sidewalls of the stripes are parallel; they were also mirror-like and separated by a 44 μ m gap. The width and height of the stripe are \sim 13.3 μ m

and $\sim 5.6 \mu\text{m}$, respectively. As such, Fabry-Pérot cavities with minimum reflection loss were obtained between the sidewalls. A schematic of a single GaN stripe on the substrate and the excitation arrangement is shown in Fig. 1(b). The signal was analyzed using a 0.32 m spectrometer equipped with a liquid-nitrogen cooled, color-coupled-detector (CCD).

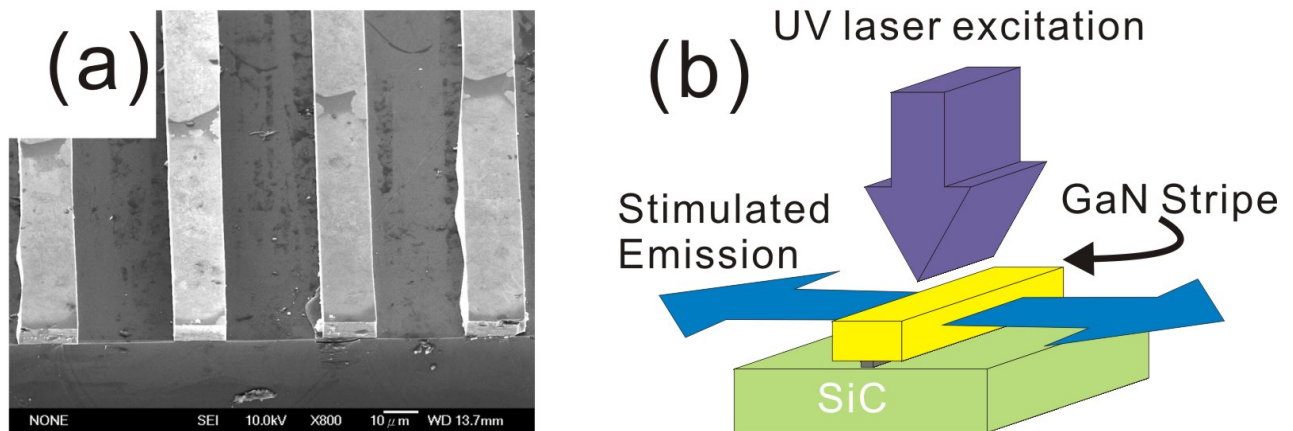


Fig 1(a) SEM micrograph of the plan-view of four uncoalesced PE-GaN stripe. The width and thickness of each stripe is $13.3 \mu\text{m}$ and $5.6 \mu\text{m}$, respectively. The sidewalls of the stripes flat and are mirror-like. (b) Schematic showing the UV excitation of one PE-GaN stripe and the resultant photoluminescence emanating from the sidewalls.

The emission spectra from a $13.3\text{-}\mu\text{m}$ -wide stripe at 77K acquired under different excitation power densities are shown in Fig. 2. A broad spontaneous emission peak was observed at excitation power densities of 2.144 and $11 \text{ MW}/\text{cm}^2$. By contrast, a set of Fabry-Pérot modes were observed located at $\sim 90 \text{ meV}$ below the bandgap energy of GaN at 77K ($\sim 360 \text{ nm}$), when the power density was increased to $38 \text{ MW}/\text{cm}^2$. Noted the band-to-band transitions maintain their spectral positions at 360 nm when the excitation power density changes. Therefore, band gap renormalization does not responsible for this below-bandgap transition. It is proposed that LO-phonon assisted processes are responsible for this transition, since the LO phonon energy in GaN is about 90 meV . The inset of Fig. 2 is an enlargement of the spectrum acquired at $38 \text{ MW}/\text{cm}^2$ and shows that the Fabry-Pérot modes are well-defined with a mode spacing of 0.6 nm . Well-defined Fabry-Pérot modes are one of the important characteristics that indicate when the lasing occurs.

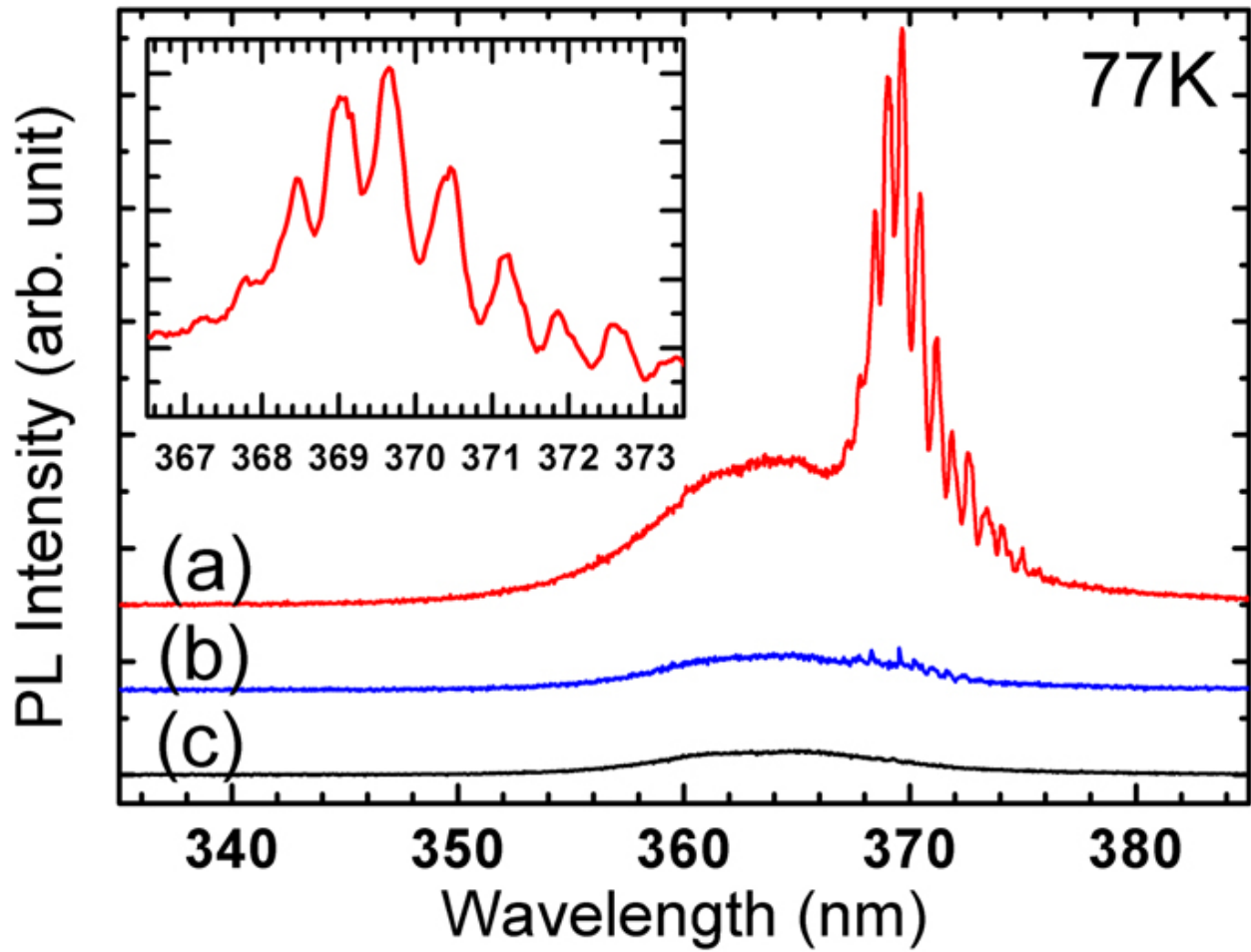


Fig. 2 Spectra of Phonon-assisted stimulated emission from a PE-GaN stripe acquired using excitation power densities of (a) 38 MW/cm², (b) 11 MW/cm², and (a) 2.144 MW/cm². Inset shows enlargement of the spectrum (a).

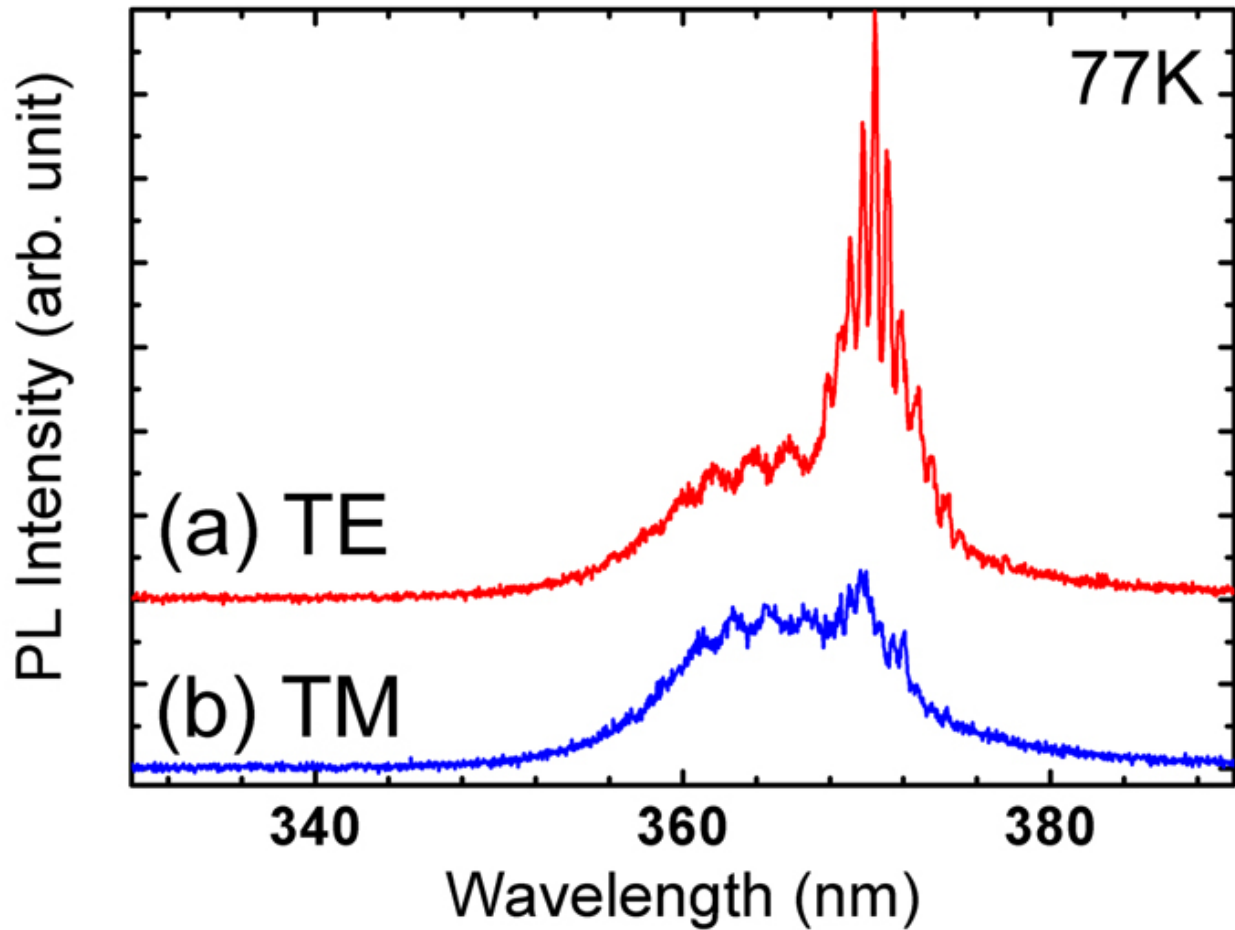


Fig. 3 (a) TE- and (b) TM-polarized emission spectra acquired at 77K using UV excitation power density of 38 MW/cm².

Photo-pumped lasing in an edge-emitting configuration favors transverse electric (TE) polarized emission, since the reflection coefficient is higher than the transverse magnetic (TM) polarization. Therefore, another key criterion that determines the occurrence of stimulated emission is the presence of a TE-polarized signal. A linear polarizer was utilized to analyze the output signal to determine the polarization of the emission signal when the excitation power density was above threshold. Only the TE-polarized emission exhibited a well-defined Fabry-Pérot mode, as shown in Fig. 3. This result verifies that these Fabry-Pérot modes located at one LO-phonon energy below the bandgap energy originate from stimulated emission of the photo-pumped GaN stripes. In addition to the phonon-assisted Fabry-Pérot modes, another set of modes with a mode spacing of 2 nm are also observed in Fig. 3. The ratio between the two sets of modes (0.6/2) is very similar to the ratio of the thickness to the width of the GaN strip (5.6/13.3). This concludes that the phonon-assisted process occurs across the width of the stripe and the other mode is the results from the cavity effects between the top and bottom interface of the thick GaN stripe.

The threshold gain, g_{th} , necessary for laser oscillation along the cavity length L may be calculated using:

$$g_{th} = \alpha + \frac{1}{L} \ln \left(\frac{1}{R_1 R_2} \right)$$

where R_1 and R_2 denote the dielectric mirror reflectivity and α is the absorption coefficient of the material. The threshold gain must overcome both the loss from the absorption of the material and the reflection of the cavity mirrors. It should be noted that the GaN stripe is uniformly illuminated across

the stripe surface and high concentration of excess carriers are uniformly generated. However, the photo-generated carriers are not uniformly distributed in the vertical direction and are concentrated within the 1 μm thick region from the sample surface for a thick 5.6 μm GaN film. Band-to-band recombination suffers a higher distributed absorption loss compared to the phonon-assisted processes and required a higher threshold gain for stimulated emission. Therefore, the threshold gain for the phonon-assisted stimulated emission (PASE) is lower than the band-to-band stimulated emission, which explains why only PASE is observed in the stimulated emission spectra.

The Fabry-Pérot mode spacing in the lasing spectra from a 13.3- μm -wide cavity has been estimated from the inset of the Fig. 3 to be 0.6 nm at the center wavelength of $\lambda_0 = 370$ nm. These data were analyzed using the following formula:

$$\Delta\lambda = \frac{\lambda_0^2}{2L \left(n - \lambda_0 \frac{dn}{d\lambda} \right)}$$

where L is the cavity length, λ_0 is the wavelength of the center mode, $\Delta\lambda$ is the spacing between adjacent modes, n is the refractive index at λ_0 and $dn/d\lambda$ is the variation of the refractive index with wavelength.

The effective refractive index $(n - \lambda_0 \frac{dn}{d\lambda})$ was calculated to be 8.578. This is a lot of different to the estimated effective refractive index (~ 4.65) from the results of spectroscopic ellipsometry measurements. [Ref. 4] The abnormal high value of effective refractive index can be partly explained by the strong distributed loss for a thick sample. In addition, it should be noted that the carrier concentration inside a material is significantly higher when stimulated emission occurs. New absorption channels related to a high carrier concentration can lead to a higher loss, which increases the value of both n and $dn/d\lambda$. As such, the value of the effective refractive index obtained from this study reflects the loss mechanisms when the carrier concentration inside an unintentionally doped GaN sample is very high. This information regarding loss mechanisms is especially important for laser diodes, since they are operating under high carrier concentrations. Understanding the loss mechanism is crucial for enhancing the efficiency of operation of a laser diode.

In conclusion, GaN stripes with mirror-like sidewalls have been grown using pendeo-epitaxial technique. Stimulated emission with well-defined Fabry-Pérot modes has been demonstrated when these PE-GaN stripes were photo-pumped at 77K. The center wavelength of the stimulated emission was located at one LO-phonon below the GaN bandgap energy, which indicates the participation of LO-phonons during the stimulated emission. This emission exhibits a preferred TE-polarization direction. An effective refractive index of 8.578 was calculated from the stimulated emission based on the cavity length and mode spacing. The high effective index refraction indicates that the absorption loss is more severe during lasing action when the excess carrier concentration is very high. Further understanding of the lasing process and phonon-assisted stimulated emission can catalyze future new developments in semiconductor laser diodes.

References:

- T. Zheleva, S. Smith, D. Thomson, K. Linthicum, P. Rajagopal, and R. F. Davis, *J. Electron. Mater.* 28, L5 (1999).
- R. M. Kolbas, N. Holonyak, Jr., B. A. Vojak, K. Hess, M. Altarelli, R. D. Dupuis, and P. D. Dapkus, *Solid State Comm.* 31, 1033 (1979).
- Y. C. Chang, Y. -L. Li, D. B. Thomson, and R. F. Davis, *Appl. Phys. Lett.* 91, 051119 (2007).
- G. Yu, G. Wang, H. Ishikawa, M. Umeno, T. Soga, T. Egawa, J. Watanabe, and T. Jimbo, *Appl.*

Growth of CNTs on Fe-Si catalyst prepared on Si and Al coated Si substrate

F.-Y. Teng, Jyh-Ming Ting*, Sahendra P. Sharma, Kun-Hou Liao

Department of Materials Science and Engineering, College of Engineering, National Cheng Kung University

*Corresponding Author. Email address: jting@mail.ncku.edu.tw

Nanotechnology 19, 095607 (6pp) Issue 9 (2008)

Carbon nanotubes (CNTs) continue to draw tremendous attentions from the entire research community since its discovery in 1991 [1]. These fascinating properties of CNTs depend on their structures, which are strongly influenced by the synthesis methods and parameters. Among the parameters, characteristics of the catalyst play a key role in controlling the structure of CNTs at molecular or nano scale. Typical catalysts that are widely employed in CNT synthesis include transition metals such as Co, Fe, Ni, Mo, and their combination such as Fe/Ni, Co/Ni, Y/Ni [2-4]. It is also known that when the formation of silicide between a catalyst and Si substrate, e.g., iron silicide, is highly undesirable. Various types of thin film materials have therefore used as an interlayer to prevent silicide formation [5-8]. In this paper, the use of a thin Al layer, ranging from 2 nm to 12 nm, between a 24-nm thick Fe-Si catalyst and a silicon substrate is reported. We show that the Al interlay not only prevents the silicide formation but also greatly enhanced the CNT growth rate at growth temperature of only 370 °C in a microwave plasma enhanced chemical vapor deposition (MPCVD) reactor. Furthermore, the use of such an Al interlayer is so effective as normally required catalyst etching prior to the growth is waived.

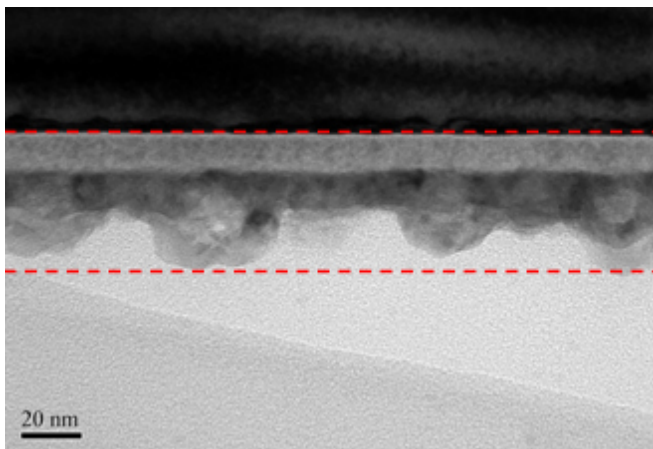


Fig. 1. TEM cross sectional image of an etched Fe-Si catalyst.

Fig. 1 shows a TEM cross sectional image of an etched Fe-Si catalyst which is bounded by the two dotted lines. It is seen that only the region near the surface become particles, adjacent to which there is a flat region. It is noted that the thickness of the catalyst layer increases from 24 nm for its as-deposited state

to 42 nm for its etched state. The flat region alone has a thickness of 12 nm. The catalyst obviously swells after the hydrogen bombardment during the etching. The surface of Al/Fe-Si catalyst also becomes particle-like after the hydrogen etching as mentioned above. However, the swelling is more severe due to the addition of an Al interlayer. For example, the thickness increases from 2 nm (Al) + 24 nm (Fe-Si) = 26 nm for its as-deposited state to 46 nm for its etched state. Notably is that the flat region alone has a thickness of 18 nm, which is almost 50% thicker than that of etched Fe-Si catalyst, i.e., 12 nm as mentioned above. Also, the Al interlayer is no longer seen. The Al is not seen in these images as it has diffused into the Fe-Si. Al was found to diffuse up to a depth of 35 nm into the Fe-Si film. Most of the Al atoms were diffused over a region of ~20 nm, limited between ~18 nm and 38 nm. For Al/Fe-Si having thicker Al interlayers, i.e., 4 nm, 6 nm, 8 nm, and 12 nm, the cross sectional morphologies and microstructure are similar to that of 2-nm-Al/Fe-Si except that the Al interlayers are visible in the 6-nm-Al, 8-nm-Al, and 12-nm-Al/Fe-Si catalysts.

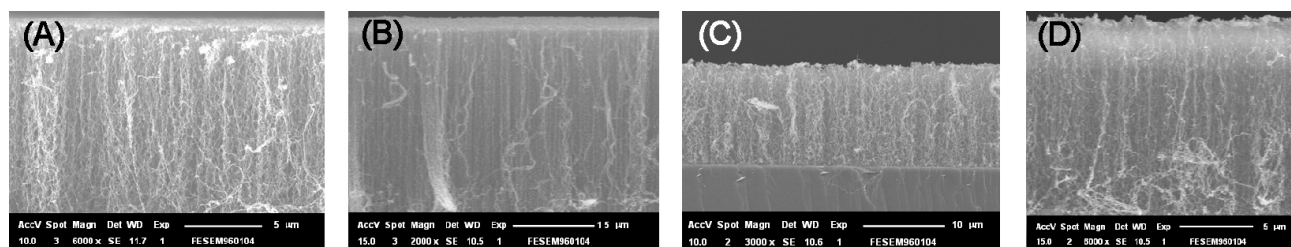


Fig. 2. SEM cross-sectional images of CNTs grown on etched Fe-Si catalysts having (A) 0-nm, (B) 2-nm, (C) 8-nm, and (D) 12-nm Al interlayers.

Figs. 2A, 2B, 2C, and 2D show SEM cross-sectional images of CNTs grown on various etched Fe-Si catalysts having 0-nm, 2-nm, 8-nm, and 12-nm Al interlayers, respectively. The methane/hydrogen ratio was 4/9. The relationship between the CNT length and the Al interlayer thickness is further shown in Fig. 3. The length of CNT increases and then decreases with the thickness of the Al interlayer. In particular, the average lengths of the CNTs grown on the Al/Fe-Si catalysts having $\sim 3 \pm 1$ nm thick Al interlayers are more than 3 times longer than that grown on the Al/Fe-Si catalysts having no Al or thicker Al interlayers. Similar effects of Al interlayer were also observed at lower methane/hydrogen ratios of 3/9, 2/9, and 1/9. Apparently there is an optimal thickness range of Al interlayer that greatly enhances the growth of CNTs. Furthermore, within this thickness range, the use of an Al interlayer is in fact so effective such that normally required catalyst etching is waived. Without the hydrogen etching, no CNT growth was observed when as-deposited Fe-Si thin films are used as the catalyst. Less effective etching of a catalyst normally occurs during the early stage of CNT growth. This allows the aforementioned swelling of the catalyst to take place and therefore the growth is enhanced. The enhanced CNT growth due to the use of a very thin Al interlayer is explained by considering the structural changes of the catalyst as mentioned above.

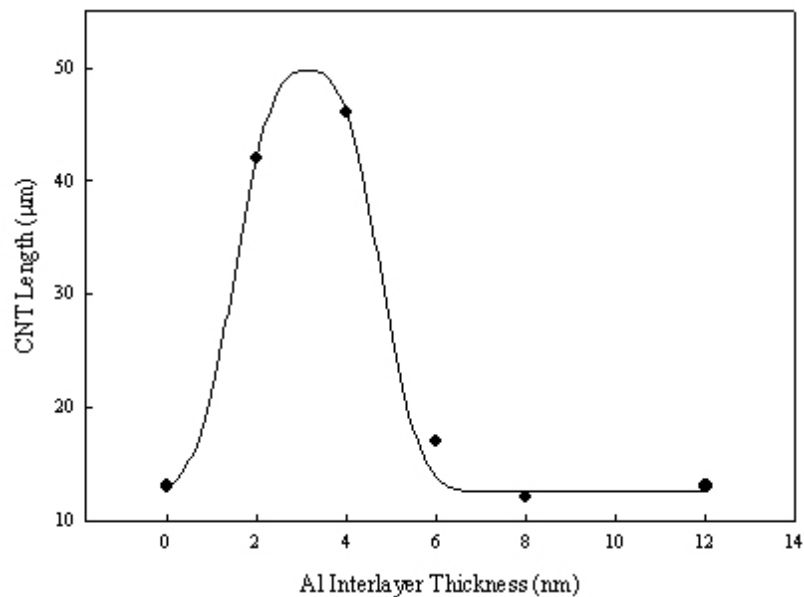


Fig. 3. CNT length increases and then decreases with the Al interlayer thickness. The methane/hydrogen ratio was 4/9.

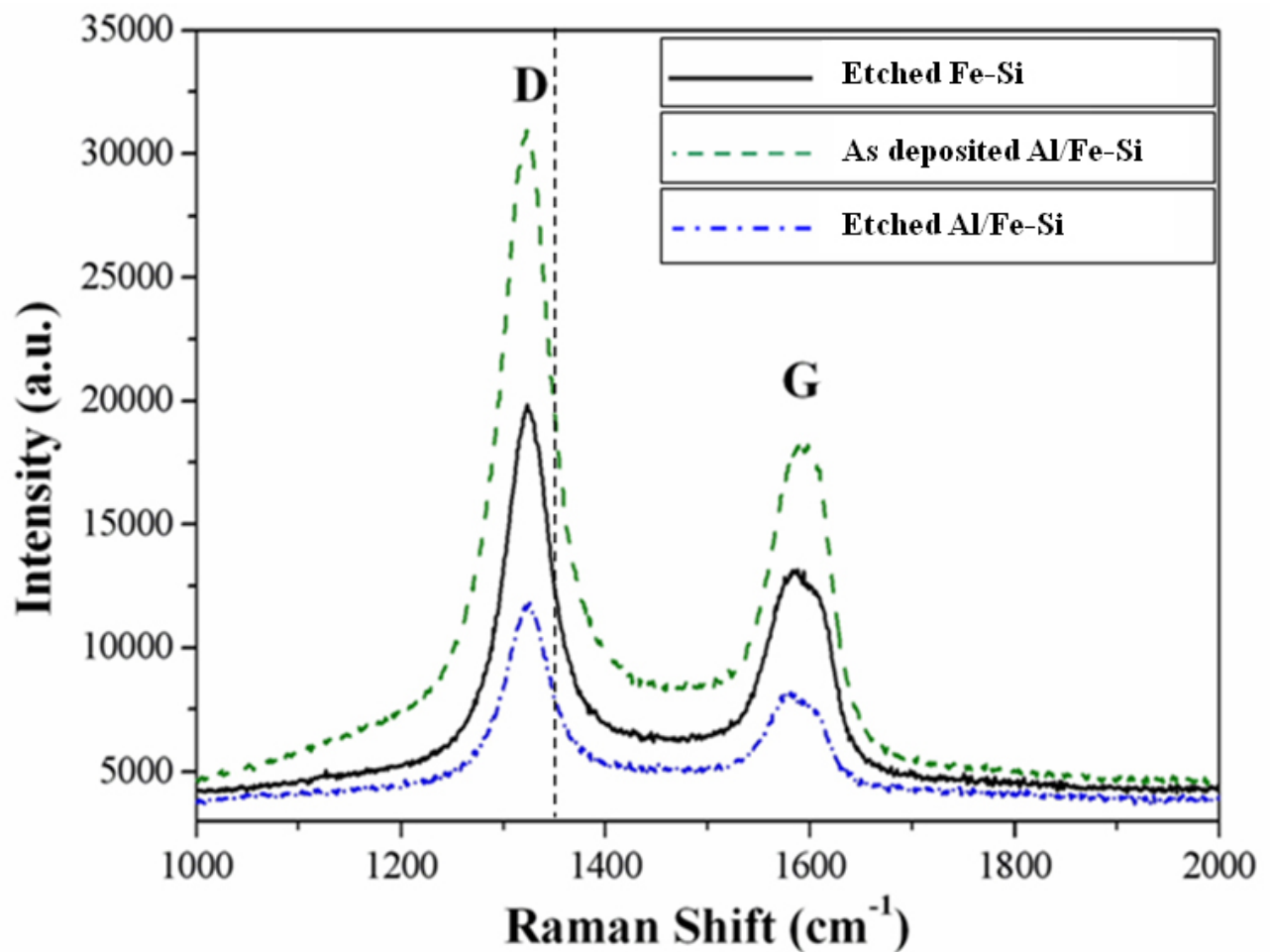


Fig. 4. Raman spectra of CNTs grown on etched Fe-Si, as-deposited Al/Fe-Si, and etched Al/Fe-Si. The methane/hydrogen ratio was 4/9.

Fig. 4 shows the Raman spectra of CNTs grown on etched Fe-Si, as-deposited 2-nm-Al/Fe-Si, and etched 2-nm-Al/Fe-Si at a methane concentration of 4/9. The Raman signatures spectra are in general similar. Commonly observed D-band and G-band are seen. However, their I_D/I_G ratios suggest that these CNTs

contains different amount of defects. The CNTs grown on the un-etched or as-deposited catalyst of Fe-Si contain the highest amount of such disorders ($I_D/I_G = 1.95$); while the defect levels of the CNTs grown on etched catalysts of both Fe-Si ($I_D/I_G = 1.50$) and 2-nm-Al/Fe-Si ($I_D/I_G = 1.55$) are less and similar. In other words, the presence of a thin layer of Al greatly enhances the growth rate of CNTs while maintaining similar microstructures for the resulting CNTs.

Conclusions

Vertically aligned CNTs have been synthesized using Fe-Si catalysts deposited on Si substrates with and without an Al underlayer at a low temperature of 370 °C. The average lengths of the CNTs grown on Al/Fe-Si catalysts having $\sim 3 \pm 1$ nm thick Al are more than 3 times higher than that grown on Al/Fe-Si catalysts having no Al or thicker Al. Within this thickness range, the use of an Al interlayer is in fact so effective such that normally required catalyst etching is waived. Such beneficial effects were observed regardless of the methane concentration used. The effects are attributed to the diffusion of appropriate amount of Al into Fe-Si catalyst which causes swelling of the catalyst, i.e., making the catalyst porous. Also, the presence of a thin layer of Al greatly enhances the growth rate of CNTs while maintaining similar microstructures for the resulting CNTs.

References

- Iijima S 1991 Nature **354** 56
- Cassel A M, Raymakers J A, Kong J and Hongjie D 1999 J. Phys. Chem. **B 103** 6484
- Chen P, Zhang H B, Lin G D, Hong Q and Tsai K R 1997 Carbon **35** 1495
- Thess A, Lee R, Nikolaev P, Dai H, Petit P, Robert J, Xu C, Lee Y H, Kim S G, Rinzler AG, Colbert D T, Scuseria G E, Tománek D, Fischer J.E and Smalley R E 1996 Science **273** 483
- Arcos T de los, Vonau F, Garnier M G, Thommen V, Oelhafen P, Düggelin M, Mathis D and Guggenheim R 2002 Appl. Phys. Lett. **80** 2383
- Delzeit L, McAninch I, Cruden B A, Hash D, Chen B, Han J and Meyyappan M 2002 J. Appl. Phys. **B 91** 6027
- Cui H, Eres G, Howe J Y, Puretkzy A, Varela M, Geohegan D B and Lowndes D H 2003 Chem. Phys. Lett. **374** 222
- Delzeit L, Chen B, Cassell A, Stevens R, Nguyen C and Meyyappan M 2001 Chem. Phys. Lett. **348** 368

Copyright 2009 National Cheng Kung University